Supporting Information

Egan et al. 10.1073/pnas.1713219114

SI Text

S1. Myosin Mathematical Modeling

The analytical approach is adapted from models of myosins interacting with an actin filament traveling x distance with steady state velocity v (44). Myosins have rate constants for attachment k_{on} (x) and detachment k_{off} (x) coupled to the state of the filament by

$$v\frac{\partial_{pon}}{\partial x}(x) = -k_{on}(x)p_{off}(x) + k_{off}(x)p_{on}(x) \quad [S1]$$

and three structural states coupled to force production f (Fig. S1).

Myosins have a rigid lever arm of length l that rotates $\theta = 30°$, relative to the myosin head, providing a linear power-stroke distance of

$$\delta_+ = l \cdot \sin(\theta) \quad [S2]$$

upon attachment. Transverse displacement a myosin head experiences is

$$\delta_o = l \cdot [1 - \cos(\theta)] \quad [S3]$$

with a myosin's stiffness κ being

$$\kappa = \frac{e_{atp}}{(\delta_+^2 + \delta_o^2)} \quad [S4]$$

where e_{atp} is a constant energy $e_{atp} = 80zJ$ extracted from ATP each cycle.

The probability a myosin is attached with displacement x_e of its head relative to its hinge is

$$p_{on}(x_e) = \begin{cases} \frac{1}{\Delta}\exp\left(\frac{x_e}{\delta_-(v)}\right) & x_e \le 0 \\ \frac{1}{\Delta} & 0 \le x_e \le \delta_+ \\ 0 & x_e \ge \delta_+ \end{cases} \quad [S5]$$

If k_{on} is a high rate of attachment that occurs only when a myosin is within a small "interaction zone" of length x_z = 1 nm, the probability of attachment is:

$$\int_0^{t_0} k_{on}exp(-k_{on}t_0)dt = 1 - exp(-k_{on}t_0) = 1 - exp\left(\frac{-k_{on}x_z}{v}\right). \quad [S6]$$

For a constant x_d = 36 nm spacing of actin binding sites, the velocity-dependent distance a binding site travels relative to a myosin per cycle Δ_c is

$$\Delta_c(v) = \frac{x_d}{1 - exp\left(\frac{-k_{on}\cdot x_z}{v}\right)}. \quad [S7]$$

The myosin duty ratio r (i.e., fraction of time attached to a filament) is

$$r(v) = \frac{\delta_{on}(v)}{\Delta_c(v)} \quad [S8]$$

and informs the time-averaged force $\langle f(v)\rangle$ of a myosin

$$\langle f(v)\rangle = \kappa \cdot r(v) \cdot x_e(v) \quad [S9]$$

where $x_e(v)$ is a myosin head's time-average displacement.

A myosin's displacement x_e upon attachment is equal to its power-stroke distance δ_+. A myosin's displacement during attachment is x_e $(v,t) = \delta_+ - v{\cdot}t$. An attached myosin produces a force of $f = \kappa{\cdot}x_e$ (v,t). The time-average displacement is

$$x_e(v) = \frac{\delta_+^2 - 2(\delta_-(v))^2}{2(\delta_+ + \delta_-(v))} \quad [S10]$$

with drag stroke $\delta_-(v) = \frac{v}{k_{off}}$, representing the negatively displaced myosin state when myosin impedes filament motility before detaching with rate constant k_{off}.

The ATPase rate

$$e(v) = \frac{v}{\Delta_c(v)} \quad [S11]$$

and power generation

$$p(v) = \langle f(v)\rangle \cdot v \quad [S12]$$

are also used to assess myosin behavior related to system performance. In Fig. S2, CS muscle myosin (l = 10 nm; k_{on} = 900 s^{-1}; k_{off} = 1,600 s^{-1}) is compared with alternate isoforms with one changed parameter value.

Alterations in myosin parameters have unique influences on the force–velocity relationship. When k_{on} is decreased, there is an increase in curvature of the force–velocity relationship; this effect has been verified with alterations in k_{on} changes that are chemically induced (54). Myosins with lower k_{off} have reduced maximum velocities, because they have a longer drag stroke and remain attached longer (43). Increases in l result in a longer power stroke that increases positive force generation and raises maximum velocity (36). Differences persist among isoforms for each parameter except for cycling rate, where only difference in k_{on} influence results.

S2. Myosin Systems Modeling

System behavior is calculated by balancing the aggregate time-average force generated by myosins for a system containing N number of myosins with loads on a given actin filament F_{app} traveling at velocity v (Fig. S3*A*). There is one solved operating velocity v_{op} that describes the system's behavior

$$F_{app}(v_{op}) = \sum_{i=1}^{N} f_i\langle(v_{op})\rangle. \quad [S13]$$

Additional myosin system behaviors include metrics for system force F_{sys} (v), the average number of attached myosins N_{att} (v), the time-average ATP use E_{sys} (v), and the system power P_{sys} (v) aggregated from contributions of all myosins at a given velocity.

In Fig. S3*B*, v_{op} differs with variations of l and F_{app}, assuming all system configuration parameters are similar to those of CS myosin. Although individual myosin stiffness decreases as l increases (55), the stalling force at the systems level remains constant since the duty ratio increases as a greater proportion of myosins are attached and contributing force.

The relative power density P_d of a system may be found with the maximum power of a system when considering all v_{op} for a given configuration, and then multiplying by the planar density

of myosins N_d divided by a packing height parameter h while additionally considering the height provided by l

$$P_d \propto \frac{P_{sys} \cdot N_d}{(h+l)} \quad \textbf{[S14]}$$

due to the uncertainty in h achievable in empirical systems, three values were considered in Fig. S3*C*. Results suggest that l longer than 10 nm (natural muscle myosin) do not significantly improve P_d for each condition.

S3. Emergent System Behaviors

The probability P that at least one myosin head is attached at a particular time for a system of N number of myosins operating at a duty ratio $r(v)$ is $P = 1 - (1 - r(v))^N$ (31). Empirical evidence suggests that systems should generally have two myosins attached on average to retain continuous functionality that occurs when P is greater than 90%. Using these criteria, there is a required number of myosin N_{req} (v) to ensure continuous functionality:

$$N_{req}(v) = \frac{2}{r(v)}. \quad \textbf{[S15]}$$

Because the energy of a system is defined as the summation of all myosins and their cycling rates (since one ATP is used per myosin cycle), and there is a minimum number of heads required for continuous functionality, it is implied that there is a minimum required energy E_{req} (v) to ensure continuous system functioning:

$$E_{req}(v) = N_{req}(v) \cdot e(v). \quad \textbf{[S16]}$$

Continuous system functioning occurs when E_{sys} $(v) \geq E_{req}$ (v), and in homogenous cases reduces to

$$E_{req}(v) \geq \frac{2 \cdot v}{l \sin\theta + v \cdot (k_{OFF})^{-1}}, \quad \textbf{[S17]}$$

which implies a critical velocity v_c that occurs when

$$E(v_c) = E_{req}(v_c) \quad \textbf{[S18]}$$

and defines the minimum filament velocity required for continuous functionality. The formulations in Eqs. **S17** and **S18** provide a basis for determining regimes of myosin system behavior when determining a critical force F_{crit} that corresponds with v_c. Considered regimes include stochastic behavior when $F_{sys} < F_{crit}$ (i.e., there is a greater than 10% chance that no myosins are attached throughout a system's lifetime), continuous behavior when $F_{crit} < F_{sys} < F_{stall}$, eccentric behavior when $F_{stall} < F_{sys}$ (i.e., when filaments are traveling in the opposite direction of the myosin power stroke), and retarding behavior when $F_{sys} < 0$. These emergent behavioral regimes are indicative of a system's robustness $Y_{sys} = F_{stall} - F_{sys}$ (v_c), where v_c does not exceed the unloaded filament velocity v_u. Relationships are plotted for a myosin system as k_{on} varies (Fig. S4).

A system has v_c lower than unloaded velocity v_u until k_{on} increases energy use such that the system is expected to operate continuously when unloaded. The robustness is equal to the magnitude of the stalling force once v_c is equal to, or exceeds v_u. Alternatively, the robustness may be increased by adding more myosins to the system.

S4. Motility Assay Experiments

CS myosin was isolated from a freshly killed chicken pectoralis muscle as described in previous efforts (56). Briefly, muscle was processed in a meat grinder that was prerinsed in 0.2 M EGTA solution and extracted on ice for 12 min in 2 mL of extraction buffer (0.3 M KCl, 0.15 M KPi, 0.02 M EDTA, 0.005 M $MgCl_2$, 0.003 M ATP, 0.005 M DTT) per gram of tissue. The reaction was terminated by adding 2 volumes of ice cold ddH_2O and filtered through a cheese cloth. Filtrate was precipitated by 10-fold dilution, 3-h incubation and centrifugation at 10,000 × *g* for 10 min. The resulting pellets were resuspended in minimal buffer and dialyzed overnight with 4 L of 0.6 M KCl, 0.25 M KPi, 0.005 M DTT at 4 °C. Actomyosin was precipitated and added to an equal volume of ddH_2O for 30 min and centrifuged at 40,000 × *g* for 1 h. Myosin was then precipitated from the supernatant by 10-fold dilution with ice cold ddH_2O. Myosin pellets were resuspended in ∼10 mL of 3 M KCl, 0.05 M KPi, 0.005 M DTT and dialyzed overnight against 0.6 M KCl, 0.05 M KPi, 0.001 M NaN_3, and 0.005 M DTT. Myosin was mixed into glycerol (50%) and stored at −20 °C until use.

Actin was prepared from chicken pectoralis muscle acetone powder. The actin was suspended in actin buffer (25 mM KCl, 1 mM EGTA, 10 mM DTT, 25 mM imidazole, 4 mM $MgCl_2$). TRITC phalloidin-labeled actin was prepared by incubating a 1:1 molar ratio of TRITC phalloidin and actin in actin buffer overnight at 4 °C. Before loading a flowcell, myosins were centrifuged in an Airfuge for 30 min at 100,000 × *g* in the presence of saturating actin and ATP (1.1 μM and 1 mM, respectively) to remove inactivated or slowly cycling myosins. A Bradford assay (Bio-Rad Labs) was used to determine myosin concentration after centrifugation. Myosin was then diluted with myosin buffer (0.3 M KCl, 0.025 M imidazole, 0.001 M EGTA, 0.004 M $MgCl_2$, 0.01 M DTT) before flow cell loading.

A flow cell channel between a nitrocellulose-coated coverslip and a standard glass slide was constructed using double stick tape (100 μm width; 3M Corp.). A concentration of myosins and α-actinin (Cytoskeleton) based on the experimental condition was then adsorbed to the coverslip surface for a 1-min incubation period. BSA (20 μL of 0.5 mg/mL suspended in myosin buffer) was introduced to the flow cell to block any remaining surface lacking myosin, and the flow cell was flushed with 20 μL of actin buffer (25 mM KCl, 25 mM imidazole, 1 mM EGTA, 4 mM $MgCl_2$, 10 mM DTT). Twenty microliters of 1 μM unlabeled actin (myosin: unlabeled actin molar ratios were ≈40:1) in actin buffer was vortexed and added to the flow cell to further minimize the influence of damaged myosin heads. After 2 min of incubation, the flow cell was washed with 40 μL of actin buffer containing 1 mM ATP followed by 80 μL of actin buffer with no ATP. Twenty microliters of 5 nM TRITC-labeled actin was then added and incubated for 1 min. Motility was initiated by the addition of actin buffer to the flow cell, which was supplemented with 0.5% methyl cellulose, 2 mM dextrose, 160 units glucose oxidase, 2 μM catalase, and saturating ATP.

A Nikon Eclipse TE2000-U microscope (Nikon) was used to observe actin filaments labeled with Tetramethylrhodamine-phalloidin at 30 °C with standard epifluoresence illumination. Image stacks were captured that consist of up to 660 frames recorded at 30 frames per second. The velocity of individual filaments in a video was found by tracking the leading edge of filaments over the course of their entire visible time for at least 200 frames, manually using the MTrackJ ImageJ plugin (57). Motility was initially checked with a filament-tracking algorithm based on centroid tracking (17, 58). For each flow cell, filament motility was recorded in several consistent locations across different samples. In most cases, at least 10 moving filaments were analyzed from at least two different areas of the flow cell to minimize surface artifact influences on measurements; if there were less than 10 moving filaments in a video, all moving filaments were tracked.

The collected empirical data (Fig. 4) enables the reverse engineering of myosin parameters for each isoform type with the model. The macromolecular structure for each myosin was assumed as l = 10 nm and θ = 30°. The detachment rate for each

isoform was found from their unloaded velocities at pure concentrations, which is about k_{off} = 1,600 s^{-1} for CS myosin and k_{off} = 250 s^{-1} for β PC muscle myosin, based on the unloaded velocity equation $v_u = \frac{\delta_+ \cdot k_{off}}{\sqrt{2}}$ (44). The attachment rate for CS myosin was assumed as k_{on} = 900 s^{-1} based on other empirical studies for CS myosin having a maximum ATPase of about 25 s^{-1}. The attachment rate of the PC myosin is then the only unknown parameter value, and was found as k_{on} = 125 s^{-1} when it was varied as an independent variable and fit to Fig. 4*D* empirical data. The lower attachment rate of the PC isoform is consistent with its lower ATPase in comparison with the CS myosin from past independent studies.

The relative isometric force of each isoform was found by holding the total myosin concentration constant and increasing concentrations of α-actinin until all filaments were stalled, which occurred at about 3 μg/mL α-actinin. The relative isometric force was found for CS and PC isoforms independently, and then in three intermediate concentrations of 1:3, 1:1, and 3:1 (Fig. S5). The *x*-axis intercept for each relative concentration was determined as an indicator of the isometric force for each isoform (i.e., the index of retardation) (48).

For heterogeneous assay experiments, the total myosin concentration was held at 100 μg/mL while relative myosin concentration varied. The 100 μg/mL concentration was found through unloaded experiments with homogenous configurations that demonstrated assays of each isoform had reached their maximum velocity once 100 μg/mL myosin was added to the system.

S5. Rule-Based Molecular Simulations

The stochastic molecular simulation provides similar predictive power to the analytical model (33), and was adapted to describe the behavior of heterogeneous myosin assays with α-actinin. A generic set of rules in Fig. S6*A* describes the three-state model of myosins and two-state model of α-actinins that do not have power strokes (i.e., they go immediately to state 2 from state 0). α-Actinins generate force-impeding motility until detaching according to a maximum displacement (Fig. S6*B*).

Myosins have a stochastic probability of attaching and detaching according to their rate constants, current state, and location of binding sites. Filament velocity is used as an independent parameter, and the resulting myosin force and cycling rates when interacting with a filament are aggregated. Results (Fig. S7) agree with the analytical model for CS myosin (l = 10 nm; k_{on} = 900 s^{-1}; k_{off} = 1,600 s^{-1}) and PC myosin (l = 10 nm; k_{on} = 125 s^{-1}; k_{off} = 250 s^{-1}).

Due to the strong agreement between the analytical and simulation models, the inclusion of simulating α-actinin is considered a means for determining α-actinin behavior that may be decoupled from myosin force contributions in experiments. Rules and parameters for describing α-actinin behavior were developed by comparing simulation results with empirical data, based on the force–balance of all molecules interacting with a single filament

$$P_{myoA} \cdot \left\langle f_{myoA}(v_{emp}) \right\rangle + P_{myoB} \cdot \left\langle f_{myoB}(v_{emp}) \right\rangle = c_{emp} \cdot P_{alp} \cdot \left\langle f_{alp}(v_{emp}) \right\rangle \quad \textbf{[S19]}$$

that includes variables describing the proportion of myosins and α-actinin (P_{myoA}, P_{myoB}, and P_{alp}), the time–average force contributions (f_{myoA}, f_{myoB}, and f_{alp}) based on the empirically measured filament velocity (v_{emp}), and experimental α-actinin concentration c_{emp}.

α-Actinin is assumed to generate force as a passive spring $f_{alp} = \kappa_{alp} \cdot e$ with stiffness κ_{alp} when displaced e distance on a filament. α-Actinins follow a two-state (attached/detached) bond rupture (49) model and detach for displacement e_{rupt}, which is consistent with their kinetic detachment rate being too low to significantly influence modeling predictions (59). For all experimental conditions, unknown parameter values were assumed across a plausible range for P_{alp} of 0.1 to 1.5, stiffness κ_{alp} of 0.5 pN/nm to 5 pN/nm, e_{rupt} of 20 nm to 40 nm, and attachment rate k_{alp} of 100 s^{-1} to 4,000 s^{-1}. A strong fit to empirical findings was reached for P_{alp} = 1.5, κ_{alp} = 2.5 pN/nm, e_{rupt} = 30 nm, and k_{alp} = 1,500 s^{-1} (Fig. 4*F*). These values are consistent with reported values of the α-actinin spring constant (59), and suggest the predictions of all molecular behaviors correspond with our modeling approaches.

S6. Homogeneous and Heterogeneous Comparisons

The analytical model is used to compare homogeneous and heterogeneous systems. Homogeneous (l = 10 nm; k_{on} = 900 s^{-1}; k_{off} = 1,600 s^{-1}) and heterogeneous systems with isoforms evenly mixed (l = 10 nm; k_{on} = 3,600 s^{-1}; k_{off} = 3,600 s^{-1} and l = 10 nm; k_{on} = 225 s^{-1}; k_{off} = 500 s^{-1}) are compared in Fig. S8 when total system size is 30 myosins.

Although they have similar force–velocity behaviors, the homogeneous system requires more myosins to retain continuous functioning when unloaded. The requirement emerges with the duty ratio of the homogenous system being lower at high velocities in comparison with the average duty ratio of the heterogeneous system. When homogeneous combinations of myosins are generated over a broad range of conditions, they have a standard nonlinear system response (Fig. S9) compared with the heterogeneous system in Fig. 4*G*.

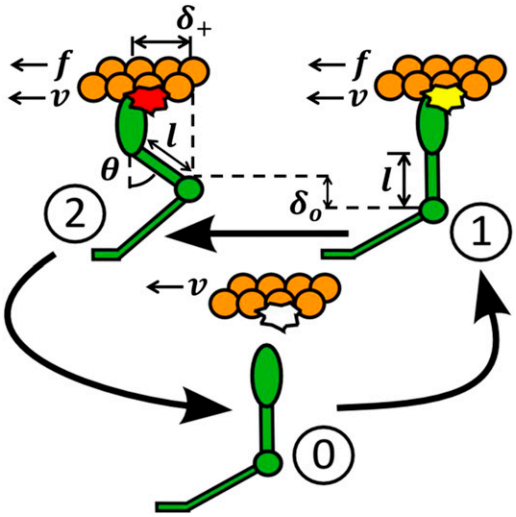

Fig. S1. Myosin mechanochemical cycle with three states (0, Detached; 1, Power stroke; and 2, Drag stroke).

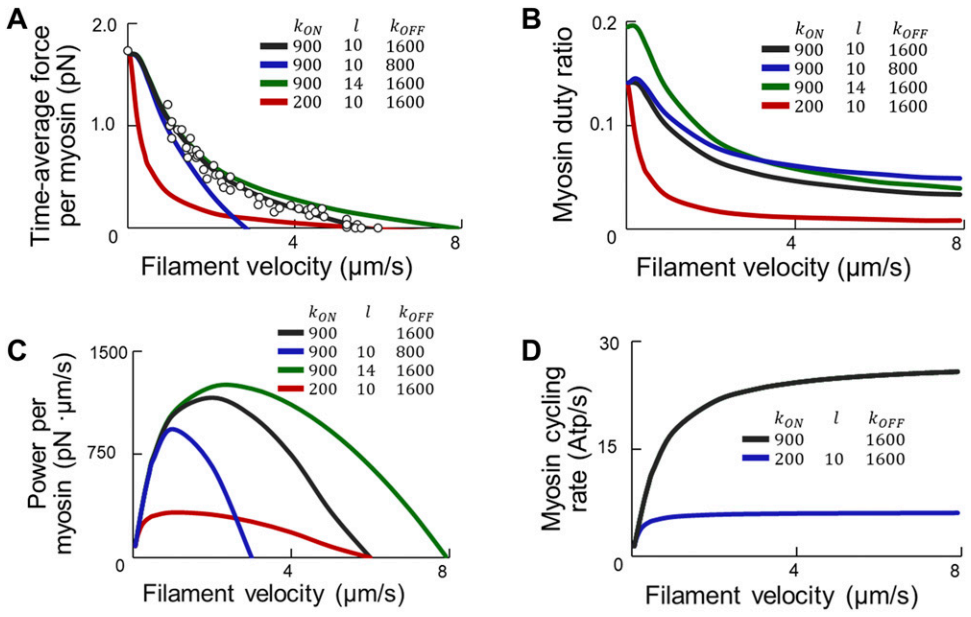

Fig. S2. Velocity-dependent behaviors of isoforms for (*A*) time-average force with overlaid empirical data (44) (*B*), duty ratio (*C*), power per myosin, and (*D*) myosin cycling/ATPase rate.

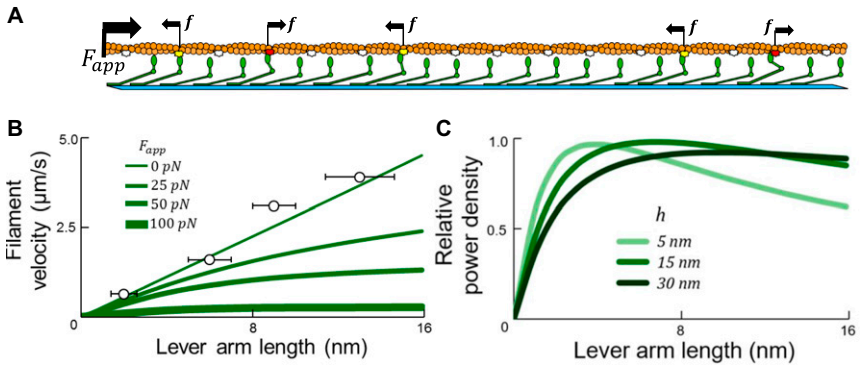

Fig. S3. (*A*) Schematic of myosin system with myosin force contributions balancing an applied force F_{app}. (*B*) Filament velocity as myosin lever arm length is varied with overlaid empirical data for the unloaded case (36). (*C*) Relative power density for systems with maximized power as packing height *h* varies.

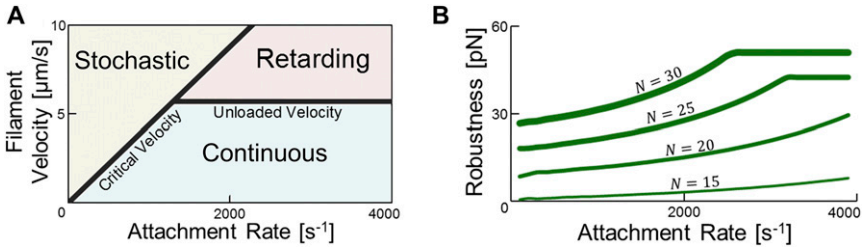

Fig. S4. (*A*) Stochastic, retarding, and concentric system behaviors for myosins of varied k_{on} and (*B*) their robustness as the number of myosins is altered.

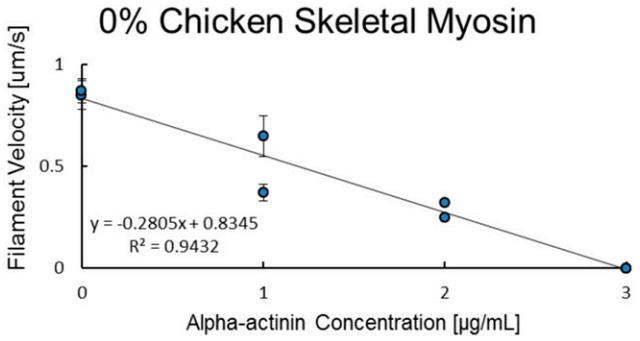

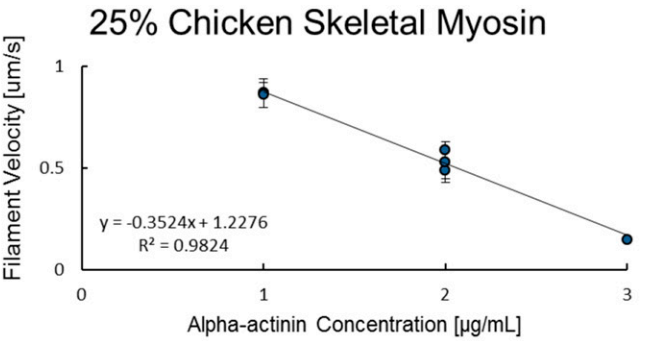

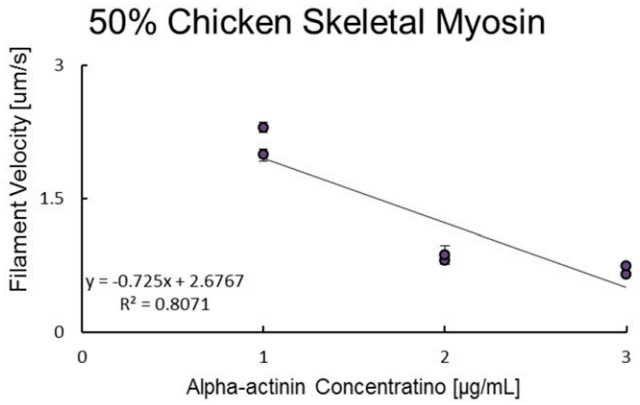

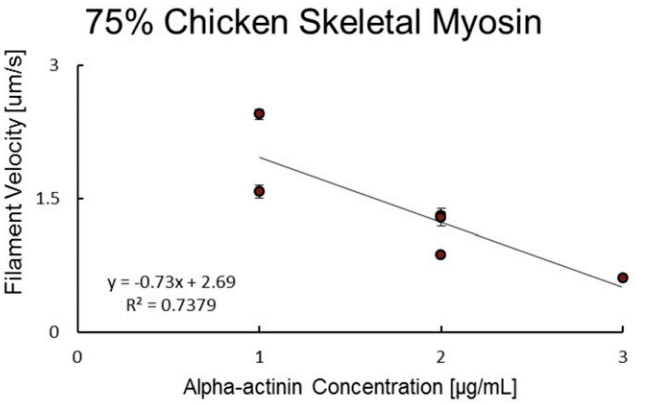

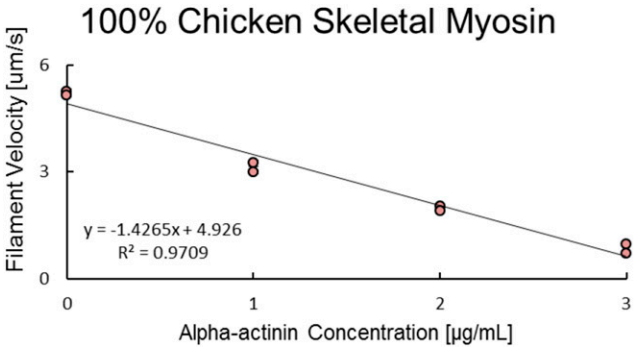

% CS	Slope	Intercept	Index of Retardation
0	-0.28	0.84	0.33
25	-0.35	1.22	0.29
50	-0.73	2.67	0.27
75	-0.73	2.69	0.27
100	-1.43	4.96	0.29

Fig. S5. Filament velocity for varied relative concentrations of CS and PC isoforms with α-actinin and their retardation indices.

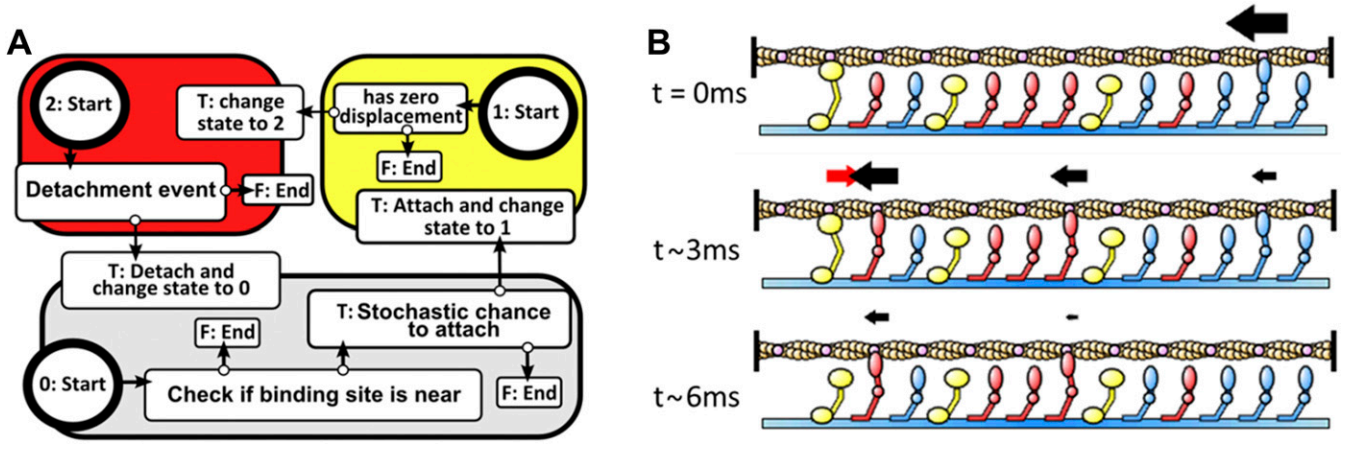

Fig. S6. (*A*) Simulation rules of molecules for each timestep and (*B*) a rendered heterogeneous system with α-actinins for a time representative of 6 ms.

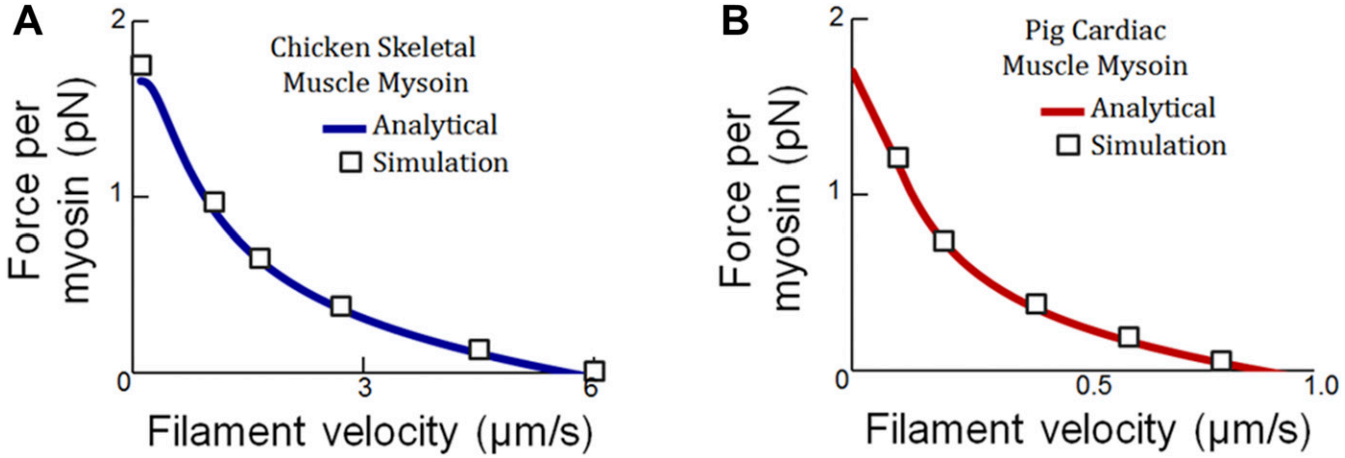

Fig. S7. Analytical model and simulation for force–velocity curves of (*A*) CS and (*B*) PC myosin.

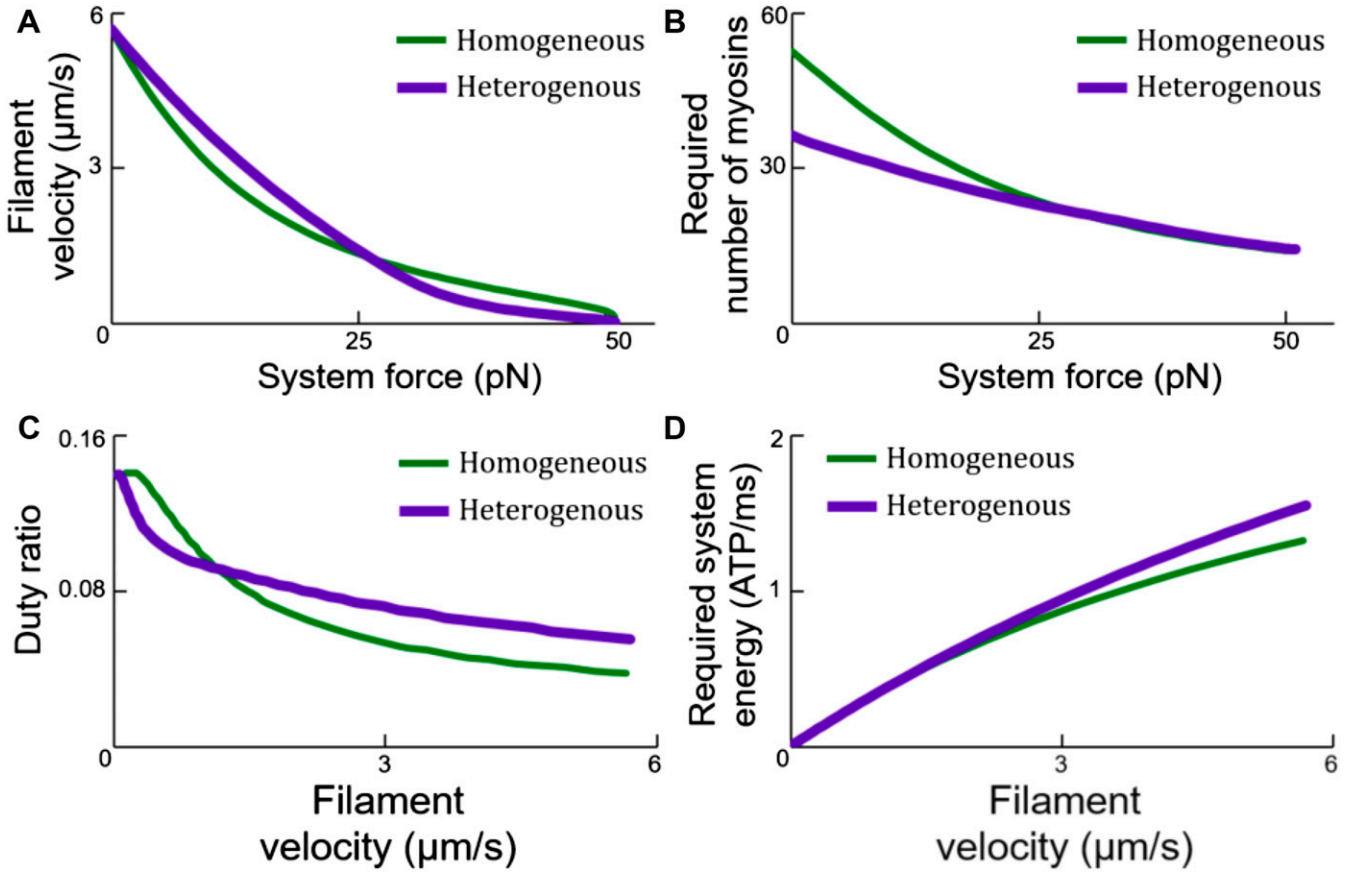

Fig. S8. Homogeneous and heterogeneous systems from Fig. 4*G* for (*A*) force–velocity, (*B*) required number of myosins, (*C*) duty ratio, and (*D*) required energy for continuous functioning.

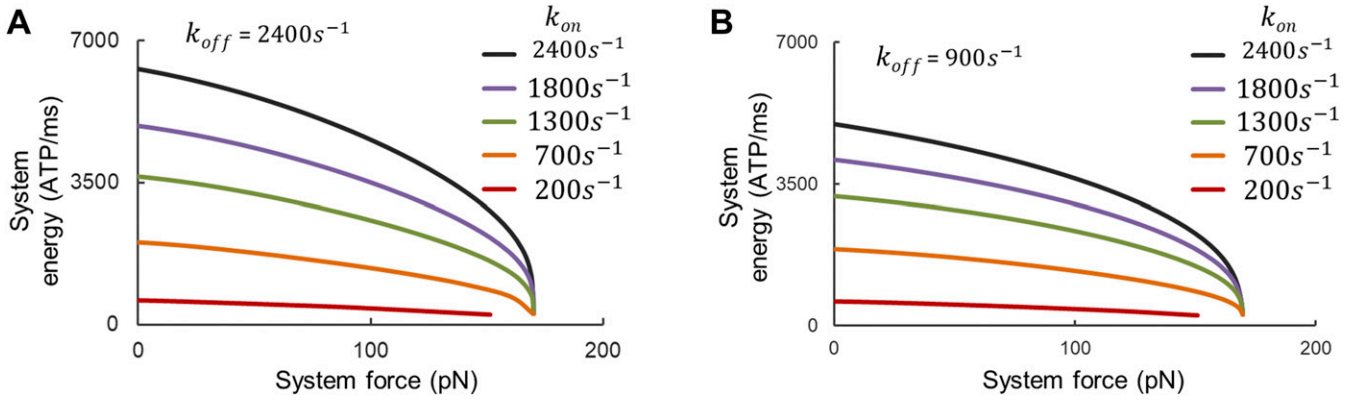

Fig. S9. Force–energy of homogeneous systems with 100 myosins of varied k_{on} when (*A*) k_{off} = 2,400 s^{-1} (*B*) and k_{off} = 900 s^{-1}.

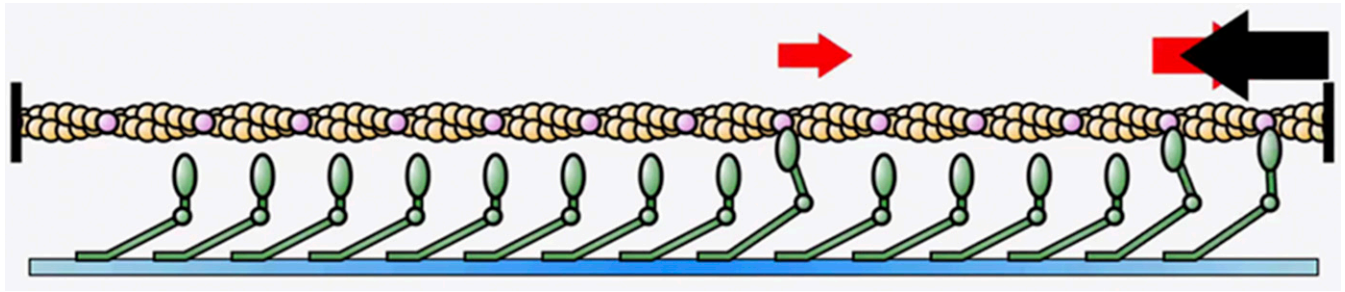

Movie S1. Myosin motility simulation: strain-dependent behaviors contributing to motility (power stroke) and impeding motility (drag stroke).

Movie S1

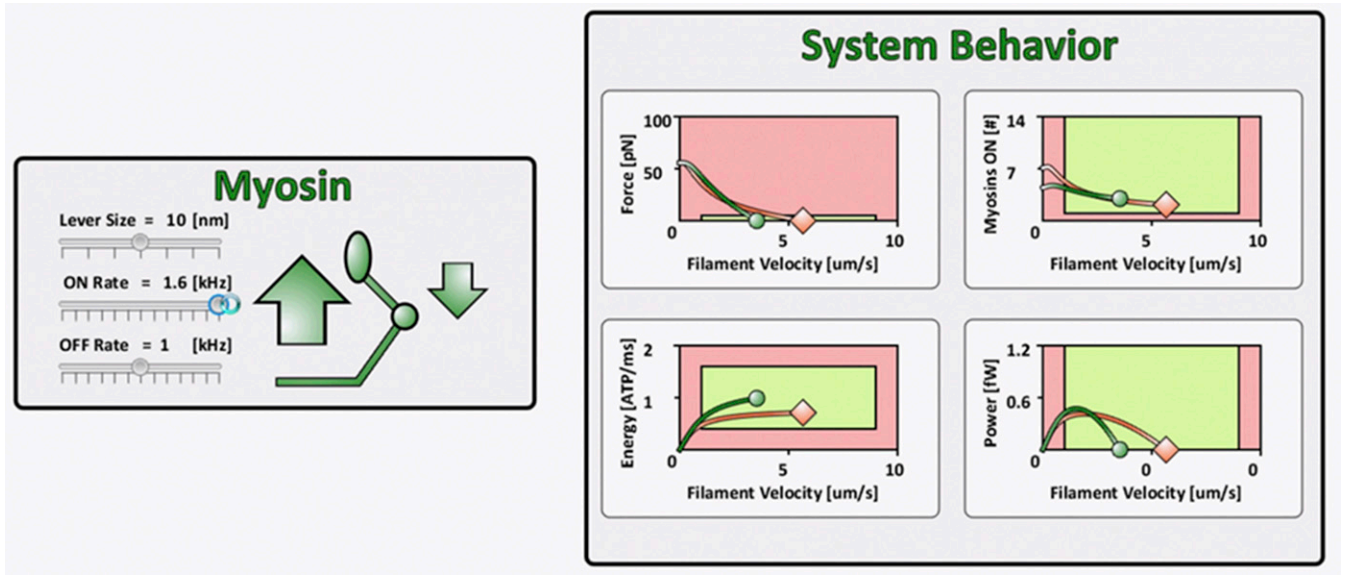

Movie S2. Homogeneous system modeling: Graphical interface with myosin parameter inputs and performance outputs.

Movie S2

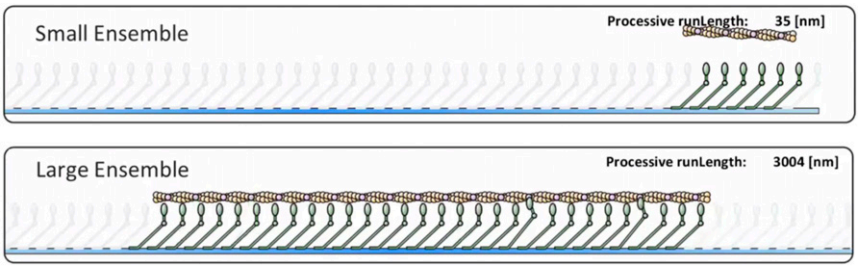

Movie S3. Motility simulation with dissociation: Simulation of filament propelled by myosins until dissociatiation.

Movie S3

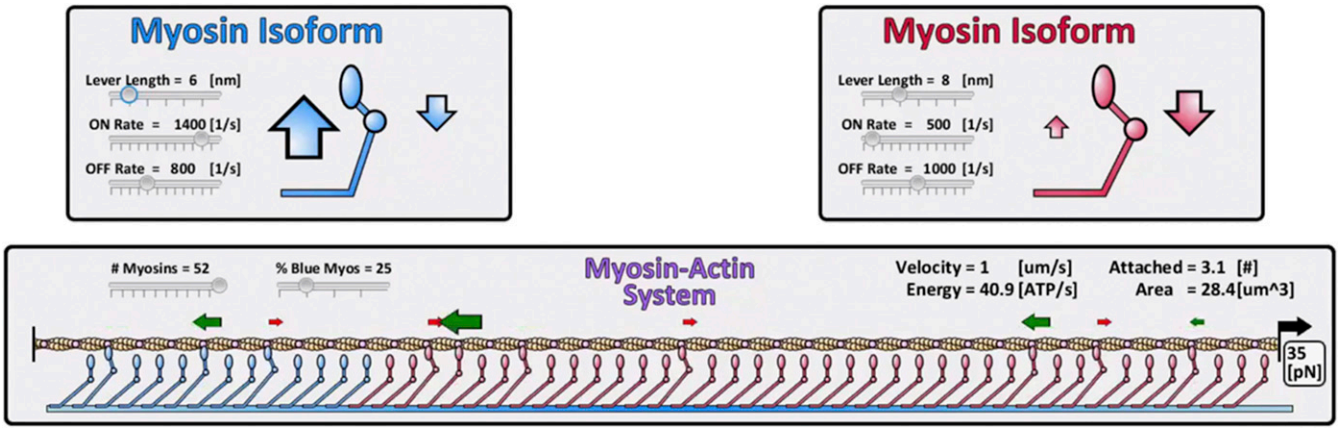

Movie S4. Heterogeneous simulation interface: Graphical interface for configuring isoforms and heterogenous systems.

Movie S4

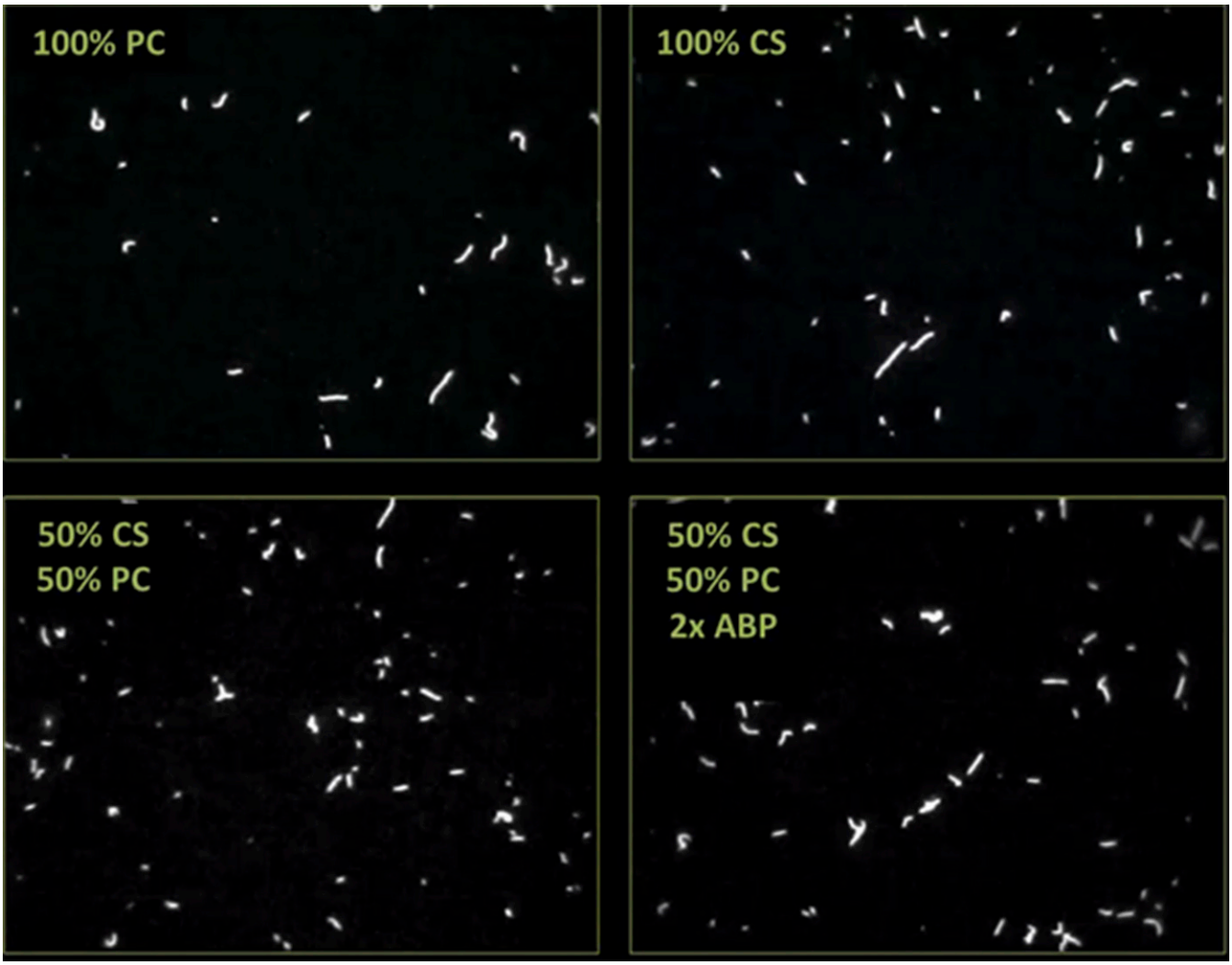

Movie S5. Motility assays (varied conditions): Microscopy of β PC muscle myosin, CS muscle myosin, and α-actinin of varied concentrations.

Movie S5

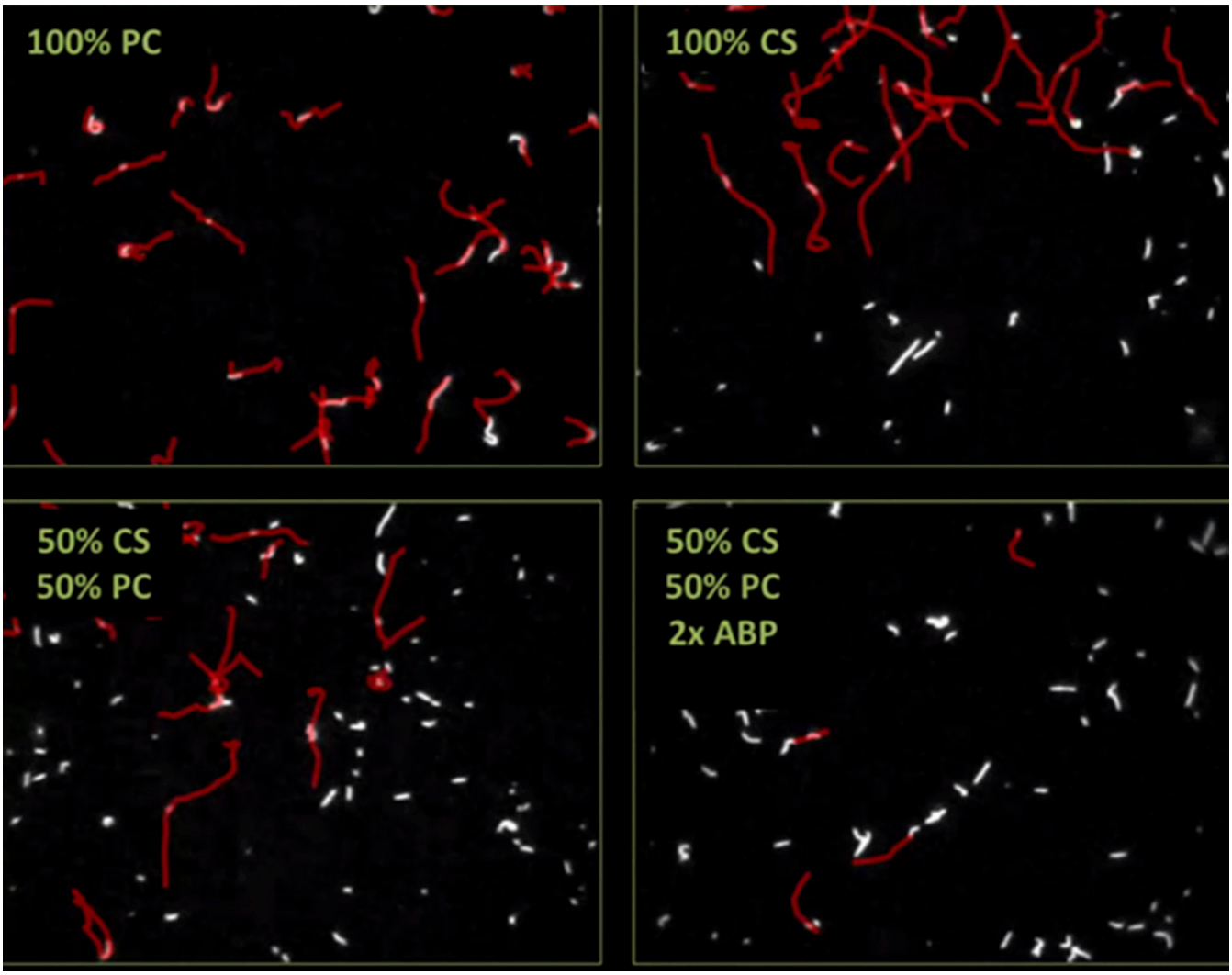

Movie S6. Motility assays (varied conditions: tracked): Microscopy from Movie S5 with motile filaments tracked.

Movie S6

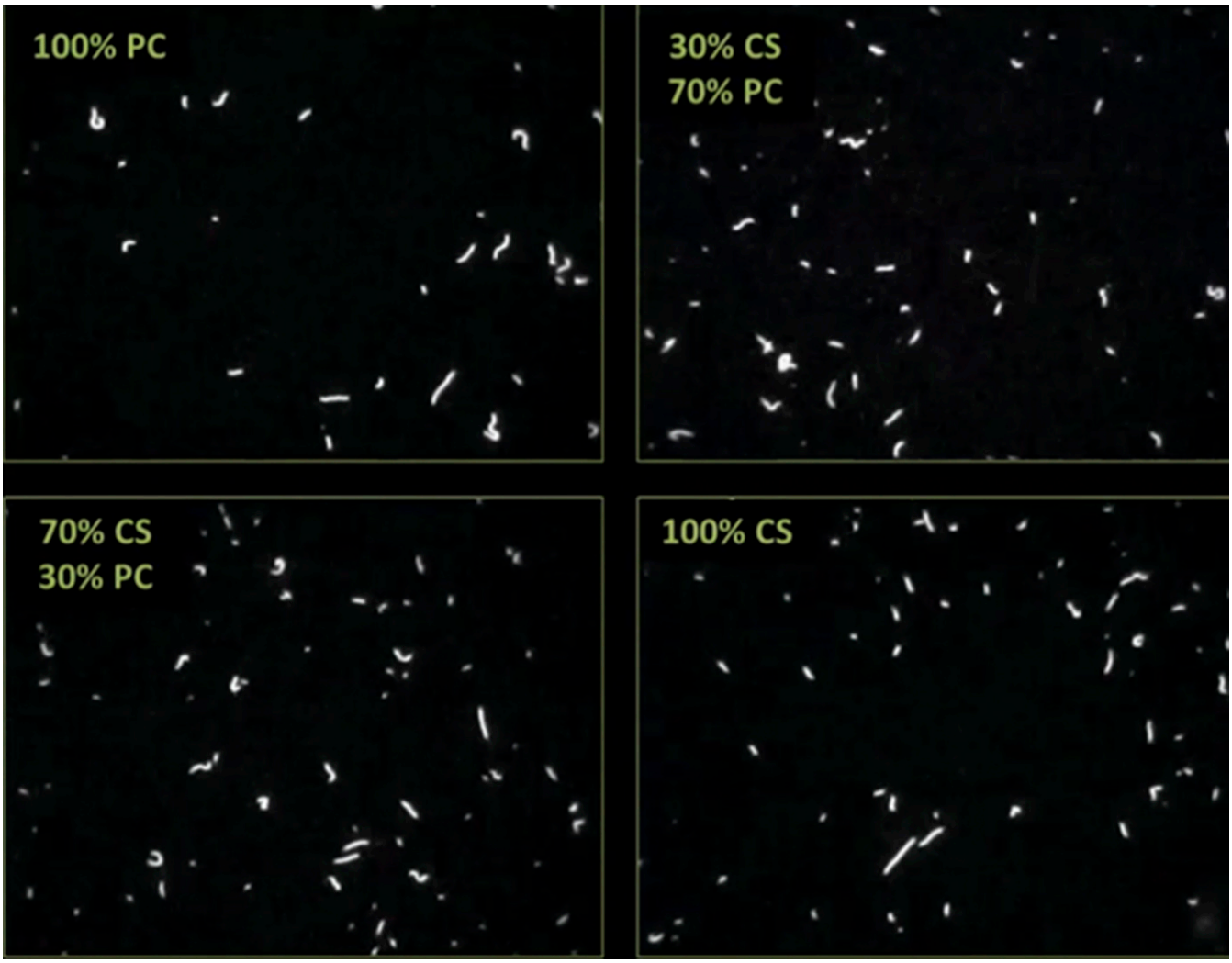

Movie S7. Motility assays (unloaded heterogeneous): Microscopy of PC and CS myosins systems of varied concentrations.

Movie S7

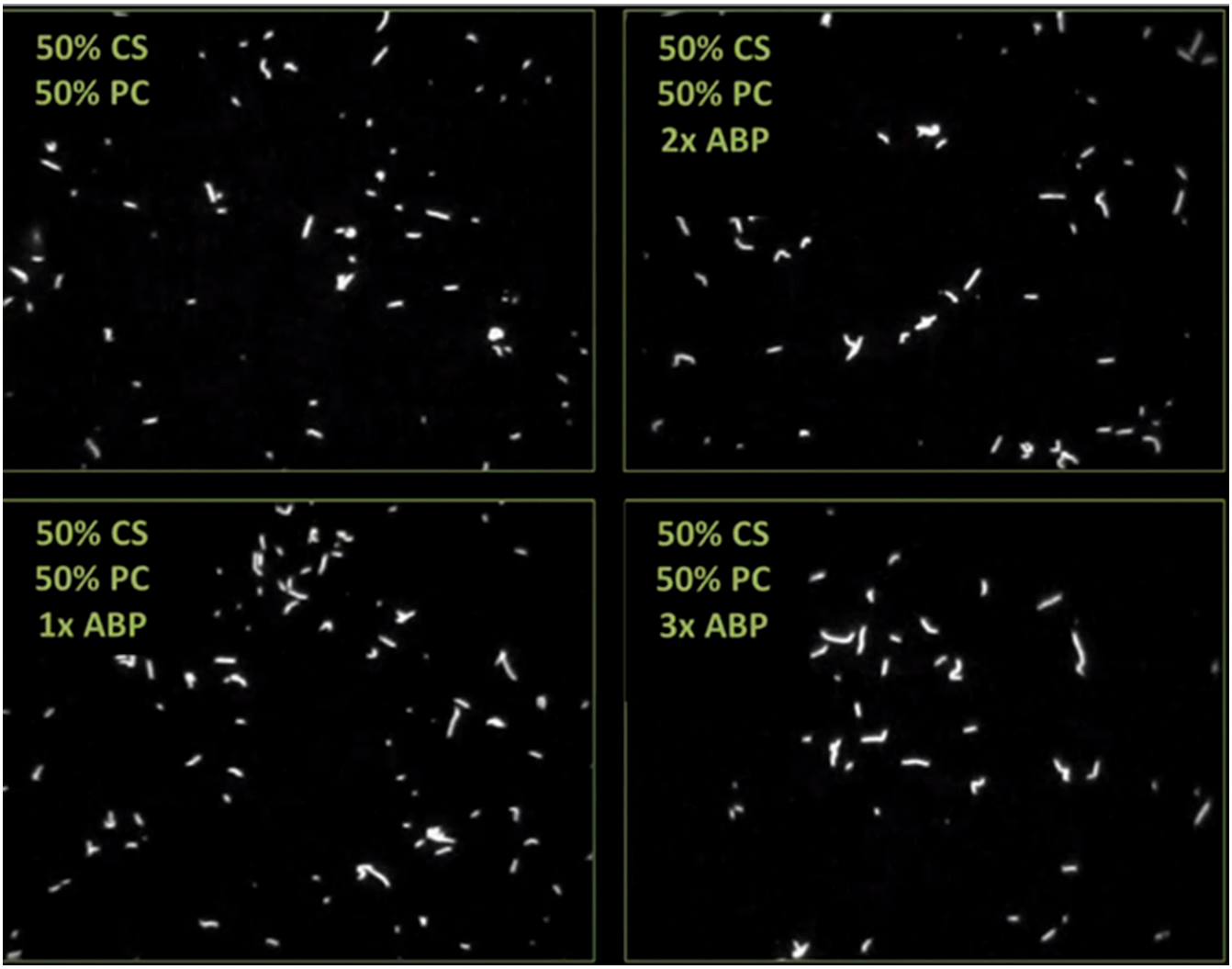

Movie S8. Motility assays (loaded heterogeneous): Microscopy of β PC muscle myosin, CS muscle myosin, and α-actinin of varied concentrations representative of loaded heterogenous experiments.

Movie S8

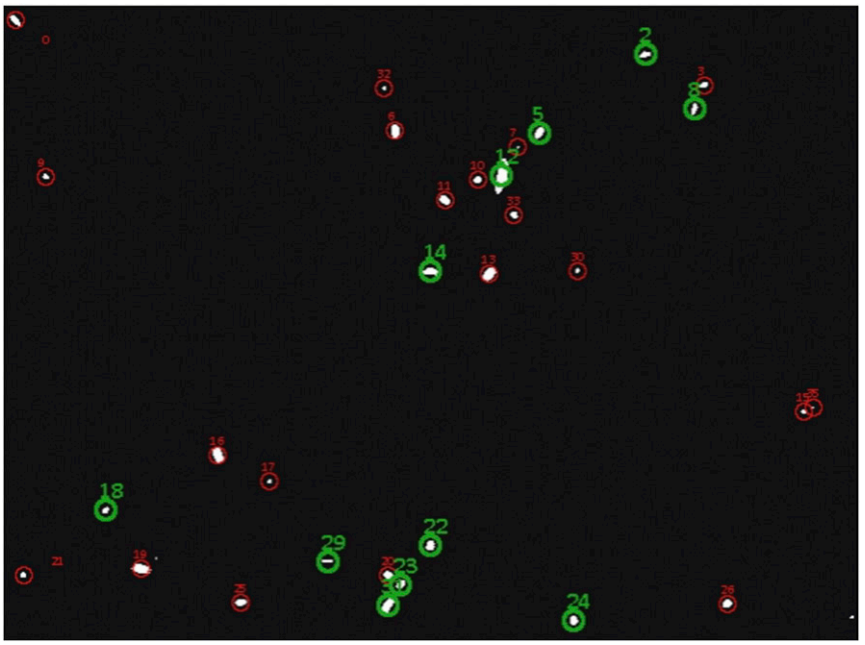

Movie S9. Automated filament tracking: Microscopy with automated filament tracking.

Movie S9

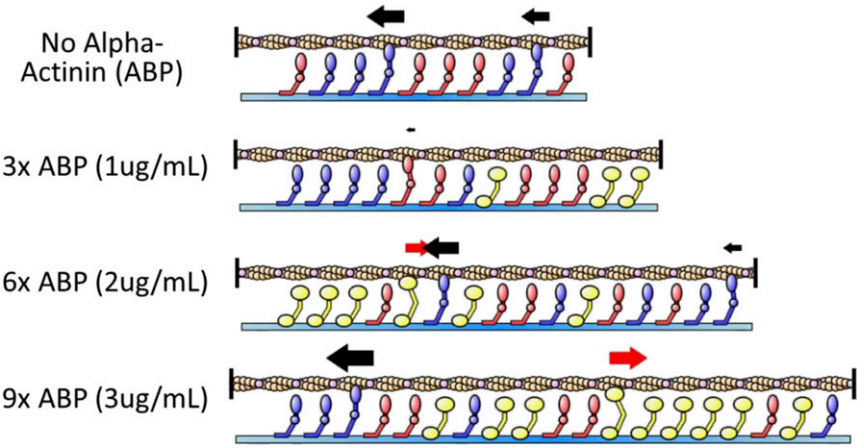

Movie S10. Loaded heterogenous simulations: Heterogeneous simulations representative of Movie S8 conditions.

Movie S10